Displacement of inactive phases by the reactive regime in a lattice gas model for a dimer-monomer irreversible surface reaction

Ezequiel V. Albano*
Instituto de Investigaciones Fisicoquímicas Teóricas y Aplicadas (INIFTA), Facultad de Ciencias Exactas, Universidad Nacional de La Plata, Sucursal 4, Casilla de Correo 16, 1900 La Plata, Argentina
(Received 17 October 1996)

A lattice gas model for the catalytic reaction $A+\frac{1}{2}B_2 \rightarrow AB$ is used for the study of the adsorbate displacement on fully covered surfaces with B and A species (i.e., poisoned phases) by the reactive state. The geometry used mimics narrow channels of width L whose ends are in contact with B_2 and A sources. Also, the channels are in contact with a reservoir of A and B_2 species in the gas phase, P_A and $1-P_A$ being the adsorption probabilities of such species, respectively. The displacement of the B-poisoned phase is slower than the A-poisoned one; however, both displacements stop at certain critical probabilities, $P_A^{c1}(L)$ and $P_A^{c2}(L)$, respectively, which depend on the channel width. Extrapolation to the asymptotic regime $L \rightarrow \infty$ leads us to conclude that such critical probabilities can be correlated with the critical points P_{1A} and P_{2A} at which the model exhibits irreversible phase transitions between a stationary reactive regime and B- and A-poisoned states. During the displacement of A-poisoned phases, it is found that the interface width $w^2(t)$ of the reactive regime diverges for $P_A \leqslant P_A^{c2}$ but remains bounded for higher P_A values. Just at the critical point one has $w^2(t) \propto t^{\beta}$, with $\beta \rightarrow 1$ for $L \rightarrow \infty$. Above the critical threshold, the time and adsorption probability dependence of w^2 is well described using general dynamic scaling arguments. [S1063-651X(97)05005-8]

PACS number(s): 82.65.Jv, 05.40.+j, 05.70.Jk, 02.50.−r

I. INTRODUCTION

Considerable effort involving both theoretical and experimental research approaches has been devoted to the study of irreversible surface reaction systems. In fact, catalytic reactions on solid surfaces are frequently of great complexity and they are thus very difficult to deal with [1]. From the theoretical point of view, there are two approaches which are widely employed: kinetic equations of the mean-field type [2] and Monte Carlo computer simulations [3]. Using the latter method, lattices are used to represent the catalytic surface. Depending on the number of different reactants and on the adsorption and reaction steps, several lattice models, such as monomer-momomer [4], dimer-monomer [5], dimer-dimer [6], etc., have been formulated and studied. Within this context, the lattice-gas version of the reaction $A+\frac{1}{2}B_2 \rightarrow AB$, as proposed by Ziff, Gulari, and Barshad [5], i.e., the ZGB model, is one of the simplest approaches to any catalytic system and, due to its interesting critical behavior, it has stimulated renewed interest in the study of irreversible phase transitions. In the ZGB model it is assumed that the reaction proceeds according to the Langmuir-Hinshelwood mechanism:

$$A(\mathrm{g})+S \rightarrow A(\mathrm{a}), \tag{1}$$

$$B_2(\mathrm{g})+2S \rightarrow 2B(\mathrm{a}), \tag{2}$$

$$A(\mathrm{a})+B(\mathrm{a}) \rightarrow AB(\mathrm{g})+2S, \tag{3}$$

where S is an empty site on the surface, while (a) and (g) refer to the adsorbed and gas phases, respectively.

The ZGB model uses a square lattice to represent the catalytic surface and the reaction is simulated by means of a Monte Carlo algorithm, which can be summarized as follows:

(i) A or B_2 molecules are selected randomly with relative probabilities, P_A and P_{B_2}, respectively. These probabilities are the relative ''effective'' impingement rates of both species, which are proportional to their partial pressures. Due to the normalization $P_A + P_{B_2} = 1$, the model has a single parameter, i.e., P_A. If the selected species is A, one surface site is selected at random and, if that site is vacant, A is adsorbed on it [Eq. (1)]. Otherwise, if that site is occupied, the trial ends and a new molecule is selected. If the selected species is B_2, a pair of nearest-neighbor sites is selected at random and the molecule is adsorbed on them only if they are both vacant [Eq. (2)].

(ii) After each adsorption event, the nearest neighbors of the added molecule are examined in order to account for the reaction given by Eq. (3). If more than one $[B(\mathrm{a}),A(\mathrm{a})]$ pair are identified, a single one is selected at random and removed from the surface.

The ZGB model is intrinsically irreversible. It is assumed that both dissociation of the dimer and reaction between a pair of adjacent species of different type are instantaneous. Also, the ZGB model basically retains the adsorption-desorption selectivity rules of the Langmuir-Hinshelwood mechanism; it has no energy parameters and the only independent parameter is P_A. Obviously, these crude assumptions imply that, for example, diffusion of adsorbed species is neglected, desorption of the reactants is not considered, lateral interactions are ignored, etc. Efforts to overcome these shortcomings have been performed by various authors

*FAX: 0054-21-254642.
Electronic address: ealbano@isis.unlp.edu.ar

 © 1997 The American Physical Society

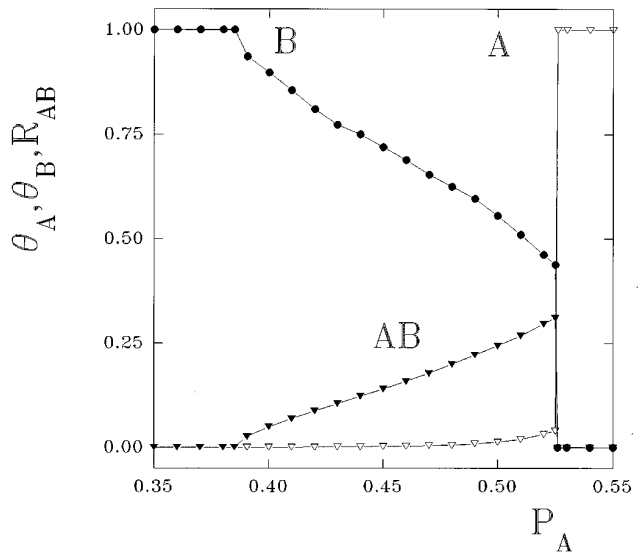

FIG. 1. Plots of the rate of AB production [R_{AB} (molecules/MCS l.u.^{2})] and the surface coverage with A (θ_A) and B (θ_B) species vs P_A for the ZGB model.

(see, e.g., [7–11]). Due to these circumstances, the ZGB model may be considered the simplest approach to describing the catalytic oxidation of carbon monoxide, i.e., A is CO, B_2 is O_2, and AB is CO_2; however, the aim of this work is to simulate a generic dimer-monomer reaction, rather than call attention to any specific reaction. In spite of the crude assumptions involved, the ZGB model exhibits a rich and complex irreversible critical behavior. In fact, in two dimensions and for the asymptotic regime ($t\rightarrow\infty$), the system reaches a stationary state whose nature solely depends on the parameter P_A. For $P_A\leqslant P_{1A}\cong 0.3906$ ($P_A\geqslant P_{2A}\cong 0.5256$), the surface becomes irreversibly covered by B (A) species, while for $P_{1A}<P_A<P_{2A}$ a steady state with sustained production of AB is observed [5]. Irreversible covered surfaces are ''poisoned'' states of the system, since it becomes inactive for further reaction. Figure 1 shows plots of the rate of AB production (R_{AB}) and the surface coverage with A (θ_A) and B (θ_B) species versus P_A. So, just at P_{1A} and P_{2A}, the ZGB model exhibits irreversible phase transitions between the reactive regime and poisoned states, which are of second and first order, respectively. Experimental evidence of a first-order ''transitionlike'' behavior has been reported for the catalytic oxidation of carbon monoxide on Pt(210) and Pt(111) [1,12]. At low enough A pressures, the rate of AB production almost vanishes and the B coverage comes close to saturation, however, the second-order transition has not been observed [1,12].

Very recently, Haas *et al.* [13] have reported experiments on the propagation of concentration fronts of adsorbed CO and O on Pt surfaces, obtained during their catalytic reaction to form CO_2. In order to avoid interference between trigger waves originating on many points of the catalyst, planar fronts are generated in narrow channels of different width (typically in the range of 7–28 μm). Each end of a channel is in contact with CO(a)- and O(a)-covered ''sources.'' Inspired by this interesting experimental work, the aim of the present manuscript is to study the displacement of poisoned phases by the reactive regime, within the framework of the ZGB model, with particular emphasis on the finite-size effects imposed by the restricted geometries of the narrow channels. In fact, it is well known that structural influences of the surface play an important role in many heterogeneously catalyzed reactions in physical, chemical, and biological processes [7,14]. The paper is organized as follows. Section II gives a brief overview of previous simulations of the propagation of concentration fronts in lattice-gas reaction systems. In Sec. III, details of the Monte Carlo simulation method are presented and relevant definitions are formulated. Section IV is devoted to the presentation and discussion of the results and the conclusions are stated in Sec. V.

II. BRIEF OVERVIEW OF SIMULATION RESULTS OF THE PROPAGATION OF CONCENTRATION FRONTS

Early Monte Carlo simulations due to Moller *et al.* [15] have demonstrated that a monomer-dimer model, which is aimed at describing the catalytic oxidation of carbon monoxide and includes reactants-assisted surface reconstruction, can support the propagation of trigger waves even if surface diffusion is not explicitly considered.

Based upon the ZGB model, Evans and Ray [16] have studied the behavior of the interface for P_A just below the first-order A-poisoning transition P_{2A}, where the interface between the reactive state and the A-poisoned one is stable [16]. Within this regime one expects that the reactive state will displace the A-poisoned one, resulting in a propagation velocity (V_p) normal to the interface. It is assumed that V_p must vanish as ($P_A\rightarrow P_{2A}$), where both states become equistables, so one has

$$V_p\propto(P_A-P_{2A})^{-\gamma}, \tag{4}$$

with $\gamma>0$. The limit of high diffusivity of the reactants can be well described by mean-field-reaction-diffusion equations, which give $\gamma=1$. It is interesting to note that if diffusion is restricted or even suppressed, simulations results give values of γ very close to unity, suggesting that the exponent is independent of the surface diffusivity of the reactants [16].

The dynamic of the propagation of the interface can be described in terms of the Kardar-Parisi-Zhang (KPZ) equation [17]:

$$\dot{h}=D\nabla^2 h+(\lambda/2)(\vec{\nabla}h)^2+\eta(\vec{r},t), \tag{5}$$

where $h(\vec{r},t)$ is the height of the interface at location $\vec{r}$ and time t. The first term of the right-hand side of Eq. (5) describes the relaxation of the interface by a surface tension D, while the second term is the lowest-order nonlinear term that can appear in the interface grow equation and accounts for the dependence of the grow rate on the local slope of the interface. In most theoretical studies, the stochastic term $\eta(\vec{r},t)$ is assumed to be Gaussian and δ-function correlated.

In the ZGB reaction system, the KPZ nonlinearity $(\lambda/2)(\vec{\nabla}h)^2$ must be present for driving the interface propagation below the transition point, however, since $\lambda\simeq V_p$, the nonlinearity vanishes [see Eq. (4)] when approaching the transition point where the interface is stationary. The presence of the nonlinear term below the transition point also requires the additional linear term [$D\nabla^2 h$ in Eq. (5)] with

$D>0$ in order to stabilize the interface propagation. Thus, D is naturally identified as the kinetic surface tension [16]. As discussed above, as the critical point ($P_A \rightarrow P_{2A}$) is approached, the nonlinearity vanishes. If D remains nonzero, then the KPZ equation will be mapped onto a linear Edward-Wilkinson equation and the interface width w in the infinite lattice is expected to behave as

$$w(t) \propto t^{\beta^*}, \tag{6}$$

with $\beta^* = \frac{1}{4}$. However, it is found that $D \rightarrow 0$ when approaching criticality and therefore one would expect $\beta^* > \frac{1}{4}$. If all linear terms vanish one may obtain the highest value $\beta^* = \frac{1}{2}$, which corresponds with the absence of any stabilizing effect. From Monte Carlo simulations at the critical point it is reported that $\beta \simeq 0.3$, i.e., a figure close to the KPZ value ($\beta^* = \frac{1}{3}$). However, this exponent indicates the operation of a weak stabilizing effect due to higher-order linear terms in Eq. (5) and these terms provide weaker stabilization mechanisms than the surface tension [16].

Very recently, Goodman *et al.* [18] have also studied the propagation of concentration waves, using the ZGB surface reaction model. It is found that the model supports trigger waves within the bistable regime of the reaction process, i.e., close to the first-order irreversible phase transition. In fact, within that regime one has the coexistence of a stable state with a metastable one. At the boundary between the two, the stable state will displace the metastable one and the boundary will move, so this process leads to the propagation of concentration fronts (trigger waves). Goodman *et al.* [18] have found that the velocity of A fronts depends on the diffusion rate of A species (D_A), B diffusion is neglected, and the sticking probability of A molecules (P_A) is determined. The velocity of the front vanishes when approaching the poisoning transition at $P_{2A}(D_A)$ (note that the critical point depends on D_A) according to Eq. (4), with $\gamma = 1$ in agreement with the results of Evans *et al.* [16]. The behavior of the interface width (w) during the propagation of the front has also been discussed in terms of the KPZ framework [see Eq. (5)] and the arguments are similar to those discussed in the previous paragraph related to the work of Evans and Ray [16]. Furthermore, the value $\beta^* \simeq 0.30$ reported by Goodman *et al.* [18] agrees with that reported by Evans and Ray [16]. In the actual catalytic system, the chemical reaction is coupled to concentration-dependent surface reconstructions [1]. Considering this effect, Goodman *et al.* [18] have also generated spiral wave patterns by means of Monte Carlo simulations, as observed in actual reaction conditions [1].

It is also interesting to compare the discussed behavior of the interface in the model (also known as the dimer-monomer process) with that exhibited by the monomer-monomer reaction for random (noninteracting) adsorption, as simulated by Kang and Weinberg [19,20]. In the monomer-monomer process, one has $\beta^* = \frac{1}{2}$, so the noise dominates over the nonlinear and surface tension terms in the KPZ equation [Eq. (5)]. In contrast, all terms of the KPZ equation have to be taken into account in the ZGB model, since here the system displays metastabilities close to the first-order critical point that are absent in the trivial, irreversible phase transition of the monomer-monomer model.

After this overview, it is useful to briefly advance the main differences between previous works and the present paper. Evans and Ray [16] and Goodman *et al.* [18] have focused their attention on the properties (mainly the interface width) of A fronts close to the first-order transition of the ZGB model, using large lattices. In this work, the displacement of unstable A- and B-poisoned phases by the stable reactive one is studied in narrow channels. Also, the velocity and fluctuations of the propagating profiles, as well as finite size effects imposed by the geometry used, are studied.

III. DETAILS OF THE MONTE CARLO SIMULATION METHOD

As suggested by the experimental work of Haas *et al.* [13], the propagation of concentration profiles during the dimer-monomer reaction is simulated using the ZGB model on the square lattice with rectangular geometries of sides $L \times M$ ($L \ll M$). So, L is the width of the channel and M is its length, and both are measured in lattice units (l.u.). Free boundary conditions are taken along the channel while the opposite ends are in contact with A and B sources, respectively. Simulations are performed running the standard ZGB algorithm, already outlined in the Introduction, but A or B species removed from the ends of the channels (the sources) due to the reaction process are immediately replaced. The propagation of the B concentration profiles are studied starting with a sample fully covered by A, except for the first column, which is covered by B (the B source), and second column, which is left empty. The propagation of A profiles are followed using a similar procedure. Under these conditions one always has two competing interfaces along the channel. The time unit is the Monte Carlo time step (MCS), defined such that each site of the lattice may have the chance to be visited once on average. Runs are typically performed until $t = 10^3 - 5 \times 10^3$ and averages are taken over 10^4 independent runs.

Figure 2 shows a set of snapshot configurations, taken at different times and obtained using lattices of size $L = 20$ and $M = 100$, corresponding to the propagation of the reactive phase (left-hand side of the snapshots) into an otherwise fully A-poisoned phase (right-hand side of the snapshots). In order to perform a more quantitative description of the propagation, a number of definitions need to be made. So, the concentration profiles of the reactants $\theta_A(x)$ and $\theta_B(x)$ are measured along the length of the channel x in the M direction and averaged over each column of lattice sites of length L. Figure 3 shows a set of concentration profiles obtained for the same times as those of the snapshots shown in Fig. 2. After determining smooth and well-averaged profiles, one can get insight into the propagation behavior by measuring the moments of the profiles which in subsequent steps can be used to determine the propagation velocity and the width of the profiles. In fact, the moments of nth order of the profiles can be evaluated according to [21]

$$\langle x^n \rangle_\theta = \frac{\sum x^n [\theta(x+1) - \theta(x)]}{\sum [\theta(x+1) - \theta(x)]}. \tag{7}$$

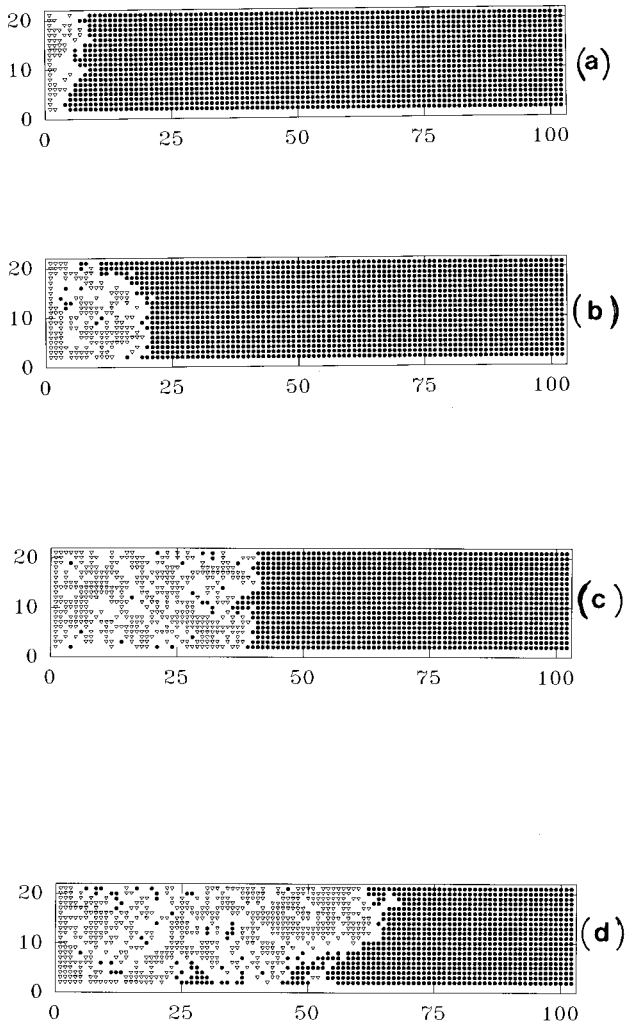

FIG. 2. Typical snapshot configurations obtained during the displacement of the A-poisoned phase (right-hand side of the figures) by the reactive phase (left-hand side of the figures). Lattice size $L=20$ l.u.; $M=100$ l.u.; $P_A=0.515$. The snapshots are plotted for different times: (a) $t=25$ MCS; (b) $t=100$ MCS; (c) $t=400$ MCS; and (d) $t=900$ MCS. Horizontal and vertical axes are measured in l.u.

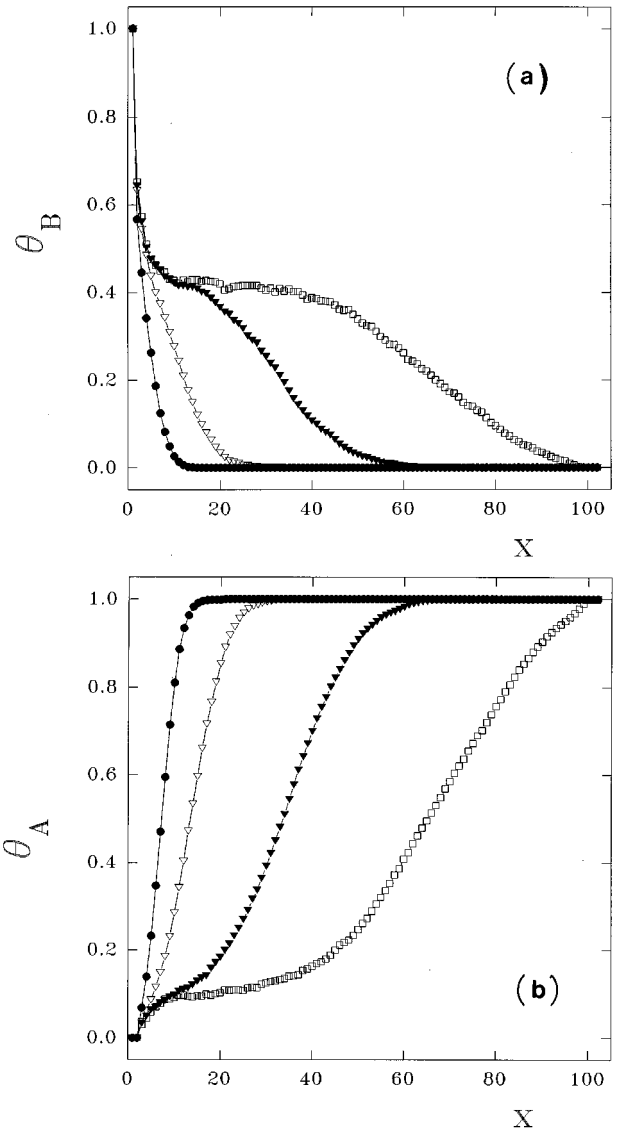

FIG. 3. Concentration profiles obtained during the displacement of the A-poisoned phase by the reactive phase. The horizontal axis is measured in l.u. Lattice size $L=20$ l.u., $M=100$ l.u., $P_A=0.515$. (a) B profiles; (b) A profiles. The profiles are plotted for different times: ● $t=25$ MCS; ▽ $t=100$ MCS; ▼ $t=400$ MCS; and □ $t=900$ MCS.

Using Eq. (7), the fluctuations in the positions of the profiles, i.e., the profile square-widths are given by

$$w^2=(\langle x^2\rangle-\langle x\rangle^2) \tag{8}$$

and the velocity of propagation can be obtained from the first moment, i.e.,

$$V=\frac{d\langle x\rangle}{dt}, \tag{9}$$

where distances are measured in lattice units (l.u.) and time in MCS.

IV. RESULTS AND DISCUSSION

A. The propagation velocity of the profiles

Starting with the first column of the channel covered by B and placed in front of an otherwise fully A-covered sample, for a high enough adsorption probability of B_2, the A-rich (unstable) phase will be displaced by the propagation of the reactive (stable) phase. This statement is illustrated in Fig. 4, which shows plots of the propagation velocity of oxygen versus the Monte Carlo time in channels of width $L=10$. For $P_A=0.467$, i.e., well inside the reactive regime, the propagation velocity quickly becomes stationary close to $V_B\simeq 0.205$ l.u./MCS. However, the speed of the propagation decreases when increasing P_A, as shown in Fig. 4 for $P_A=0.490$ with $V_O\simeq 0.105$ l.u./MCS. Furthermore, at a certain critical threshold P_A^{c2} such propagation will stop, see Fig. 4 for $P_A=0.512$ where, after some short transient period, V_B vanishes.

Again, starting with a column covered by A in an otherwise B-poisoned phase, the stable reactive state will displace the unstable poisoned state, but now the speed of propaga-

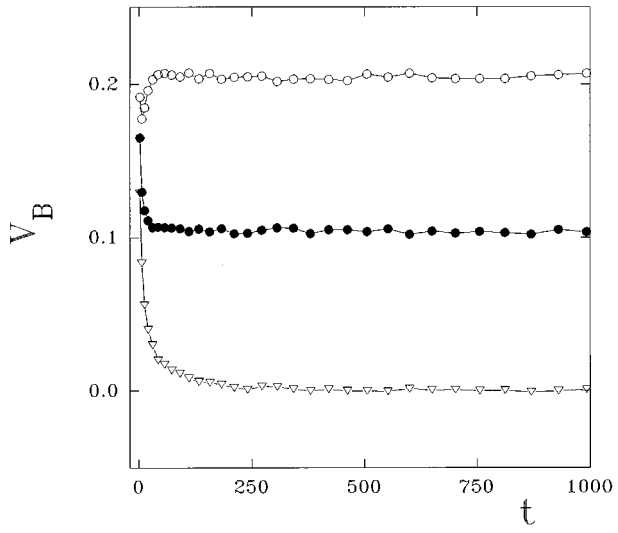

FIG. 4. Plots of the propagation velocity of B profiles v_B (l.u./MCS) vs t (MCS) measured in channels of width $L=10$. Upper curve $P_A=0.467$, medium curve $P_A=0.490$; and lower curve $P_A=0.512$.

tion will decrease when decreasing P_A, and at the threshold P_A^{c1} the propagation will stop. Between both thresholds the coexistence of A and B propagating profiles is observed and the study of their properties is the goal of this section.

Figure 5 shows plots of the steady-state velocities, as defined by Eq. (9), versus P_A. For a very narrow capillary [$L=3$, Fig. 5(a)] the propagation of A and B profiles stops at the critical probabilities $P_A^{c1}(L=3)\simeq 0.438$ and $P_A^{c2}(L=3)\simeq 0.451$, respectively. So, in this case the propagation of both profiles can only coexist within a narrow window of width $\Delta P_A\simeq 0.013$. Increasing the width of the channel [Fig. 5(b) with $L=10$], one observes the shift of both critical probabilities, which are now located at $P_A^{c1}(L=10)\simeq 0.412$ and $P_A^{c2}(L=10)\simeq 0.512$. Accordingly, the width of the coexistence window increases up to $\Delta P_A\simeq 0.100$, but this effect is mostly due to the shift of P_A^{c2}. Also, close to P_A^{c2}, when the propagation of the B profile ceases, the speed of the A profile undergoes a sharp increase. This behavior can be correlated with the first-order irreversible phase transition between the stationary reactive regime and the A-poisoned state, which is observed in the ZGB model at P_{2A} (see Fig. 1). In fact, the propagation velocity of the A profile within the A-poisoned state must be faster than that measured within the reactive regime, in accordance with the abrupt increase of the coverage with A species observed at the critical point. So, the critical probability at which the B profile stops its propagation can be correlated with the critical point of the first-order transition of the ZGB model.

Figure 6 shows plots of the critical pressures $P_A^{c1}(L)$ and $P_A^{c2}(L)$ versus the inverse of the channel width L^{-1}. It is found that in the $L\to\infty$ limit these probabilities converge to the critical points at the second- and first-order irreversible phase transitions of the ZGB model, respectively. So, coexistence of propagating profiles occurs within the reactive window limited by the critical points. The marked dependence of the coexistence window on the channel width reflects the strong finite-size effect imposed by the underlying geometry.

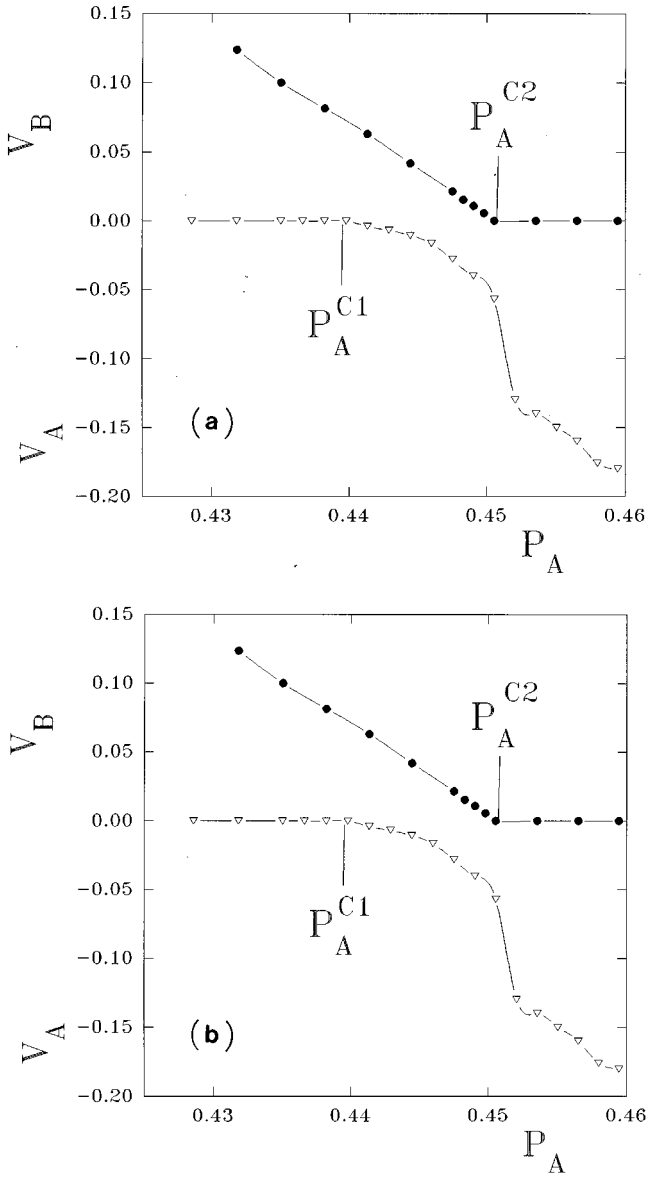

FIG. 5. Plots of the propagation velocities of B and A profiles vs P_A obtained for channels of width (a) $L=3$ l.u. and (b) $L=10$ l.u. The lines show the critical probabilities at which propagation stops.

The main results of the simulations can be summarized as follows: (a) two critical probabilities $P_A^{c1}(L)$ and $P_A^{c2}(L)$, which depend on the width of the channel, at which the profile propagation stops are found; (b) within these critical values, coexistence of A and B propagating profiles is observed; (c) the propagation of B profiles is faster than that of the A ones. All these observations appear in qualitative agreement with the experimental results reported in Fig. 2(a) of the paper of Haas *et al.* [13]. However, the underlying physics is different: in the simulations, the displacement of a poisoned phase by the invading reactive phase takes place within a range of adsorption probabilities where the latter is unstable while the former is stable. In contrast, the experiment may show the propagation of coexisting phases within a bistable regime [13]. As discussed above, the simulations

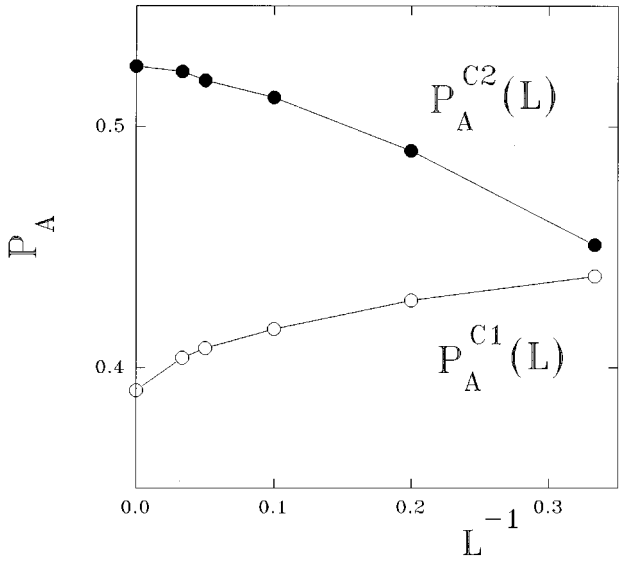

FIG. 6. Plots of the critical probabilities $P_A^{c1}(L)$ and $P_A^{c2}(L)$ at which propagation of A and B profiles stops, respectively, vs the inverse of the channel width L^{-1} (l.u.$^{-1}$). The points at $L=\infty$ are P_{1A} and P_{2A}, respectively.

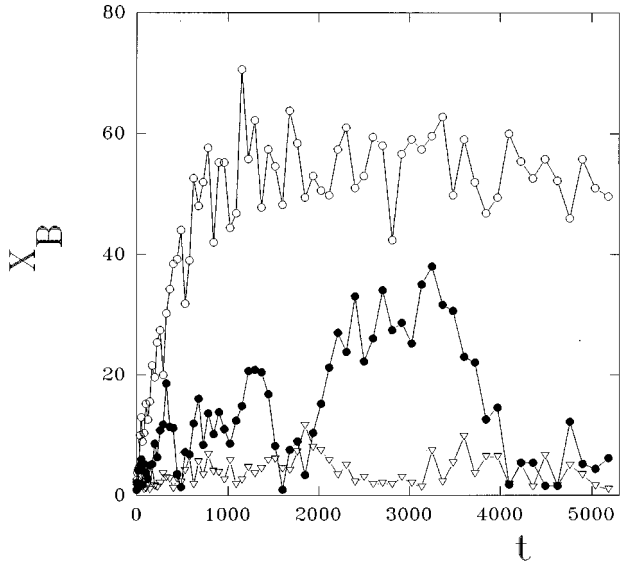

FIG. 7. Plots of the position x_B (l.u.); of a single oxygen profile vs t (MCS), obtained with a lattice of size $L=5$ l.u., $M=100$ l.u. and for different adsorption probabilities close to the critical probability $P_A^{c2}(L)\simeq 0.4852$. ○ $P_A=0.474$, ● $P_A=0.485$; and ▽ $P_A=0.500$.

also show a jump in the velocity of A fronts that occurs close to $P_A^{c2}(L)$. In the experiments A fronts are not studied above P_A^{c2}, so the occurrence of the jump in actual conditions cannot be ruled out. The occurrence of that jump may be a nice prediction of the (simple) ZGB model, which, in principle, seems to be supported by the fact that the jump can effectively be correlated with the first-order poisoning transition, and a first-order transitionlike behavior has already been observed experimentally [12].

While displacements of coexisting phases can occur within the whole reactive regime, this phenomenon becomes particularly interesting close to the first-order transition, where metastable behavior is observed. In fact, close to the first-order irreversible phase transition, between the lower spinodal point and the critical point, to be more precise, one has a metastable A-poisoned state which coexists with a stable reactive state. At the boundary between both states, the stable state will displace the metastable one and the boundary will move. However, due to the stochastic nature of the underlying process, and also favored by the finite width of the channel, the boundary may remain unbounded, undergoing backward and forward excursions. Under these conditions, reflection of B fronts close to $P_A^{c1}(L)$ may be observed. Figure 7 shows the time dependence of the positions of the centers of B profiles, obtained in a single simulation with a channel of width $L=5$ and for three different adsorption probabilities. For $P_A=0.500>P_A^{c2}$, the B profile remains bounded and cannot propagate into the A-poisoned phase. For $P_A=0.474<P_A^{c2}$, the reactive phase can effectively displace the A-poisoned one, as evidenced by the quick change in the profile position observed for $t<1000$. Later on, the phase remains bounded close to the end of the channel, which has been set at $M=80$ in order to see this effect. Finally, for $P_A=0.485\simeq P_A^{c2}$, i.e., within the bistable regime, the excursions of the profile can easily be observed.

B. The behavior of the profile's width

It is well known that lattice-gas modeling of surface reactions, in contrast to traditional mean-field treatments, provides a realistic description of the fluctuations and correlations resulting from the adsorption and reaction processes. In a deterministic process described by a set of reaction-diffusion equations, the interface between coexisting phases may have a fixed width [18]. Such width should be on the order of the size of the region near the propagating front. In contrast, in the lattice-gas description, shot noise in the pressure of the incoming reactants and statistical fluctuations are extra sources of broadening, which leads to wandering of the front [18]. Due to these circumstances, and in order to gain a deep understanding of the phase-displacement process, the fluctuations in the position of the center of the profiles, as defined by Eq. (8), are investigated. This quantity includes the fluctuations in the front as well as in the coverage near the front.

Figure 8 shows the dependence of the fluctuations in the position of the center of B profiles (i.e., the interface width) as a function of time obtained for channels of different width and at various adsorption probabilities, when the A-poisoned phase is displaced by the reactive phase. Two different regimes can clearly be observed. For low P_A values, well inside the reactive state, the fluctuations diverge and the poisoned state will ultimately be completely displaced. For high enough P_A values, well inside the A-poisoned state, the fluctuations saturate, i.e., the reactive state cannot displace the stable poisoned state and the interface remains bounded. The crossover between these two regimes is observed just at the critical probability $P_A^{c2}(L)$ where log-log plots of w_L^2 vs t give straight line behavior. So, based on general dynamic scaling arguments, similar to those used to describe the interface fluctuations upon thin film growth [22], it can be expected that the stochastic evolution

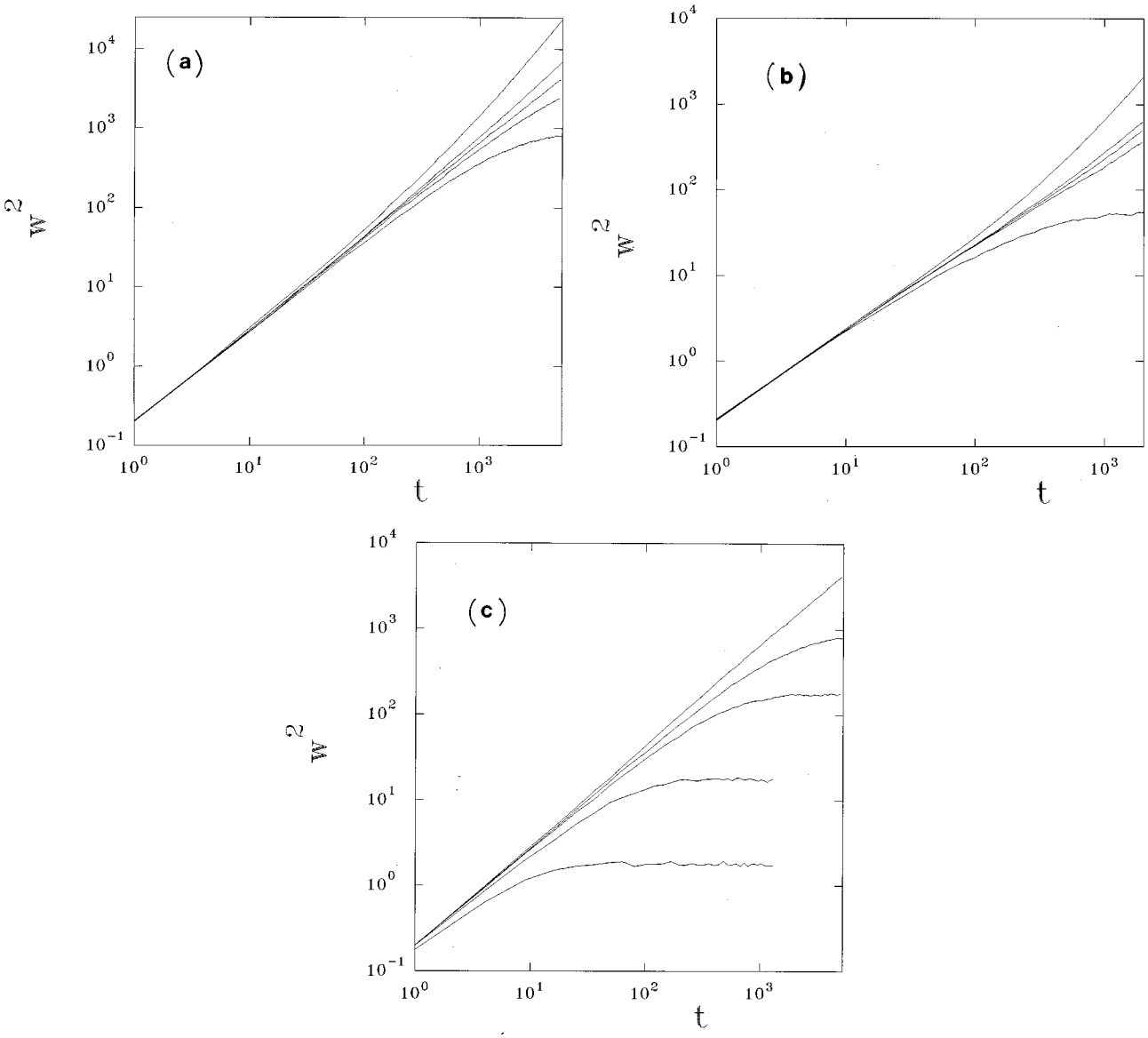

FIG. 8. Log-log plots of w^2 (l.u.^{2}) vs t (MCS), measured at different adsorption probabilities and for channels of different width. Data obtained during the displacement of an A-poisoned phase by a reactive phase. (a) $L=5$ l.u., from top to bottom the probabilities are 0.4819, 0.4845, 0.4852, 0.4859, and 0.4872; (b) $L=30$ l.u., from top to bottom the probabilities are 0.5192, 0.5202, 0.5211, 0.5215, and 0.5238; and (c) $L=5$ l.u., from top to bottom the probabilities are 0.4852, 0.4872, 0.4898, 0.5000, and 0.5349.

of a driven interface along a strip of width L may be characterized by long-wavelength fluctuations $[w_L^2(t,\Delta P_A)]$, which have the following time and P_A dependence [22]:

$$w_L^2(t,\Delta P_A)\propto t^{\beta}F(t(\Delta P_A)^{\alpha}), \tag{10}$$

where $\Delta P_A=P_A-P_A^{c2}(L)$, with $F(x)=$ const for $x\to 0$ (i.e., $\Delta P_A\to 0$) and $F(x)\to x^{-\beta}$ for $x\to\infty$ (i.e., $\Delta P_A>0$ and $t\to\infty$). Thus, just at the critical pressure, the time divergence of the fluctuations is given by $w_L^2(t)\propto t^{\beta}$ as $t\to\infty$, while off-criticality, the fluctuations may diverge according to $w_L^2(\Delta P_A)\propto\Delta P_A^{-\delta}$, with $\delta=-\alpha\beta$. Note that $\beta^*=\beta/2$, where β^* has been defined in Eq. (6).

From log-log plots of w_L^2 vs t (see Fig. 8), one can accurately determine both the critical probability and the exponent β. The obtained results are summarized in Table I. While for narrow channels β depends on L (i.e., nonuniversal behavior is observed), increasing the channel width by one has $\beta\to 1$ for $L\to\infty$. In spite of the fact that the KPZ arguments, summarized in Eq. (5), do not strictly apply because the measured interface width includes the fluctuations

TABLE I. Critical probabilities and critical exponents. The error bars merely reflect the statistical error.

L	P_A^{crit2}	β	δ
3	0.4498(3)	1.24(2)	1.98(1)
5	0.4852(3)	1.17(2)	1.88(1)
10	0.5086(3)	1.13(2)	
20	0.5186(3)	1.03(2)	1.65(3)
30	0.5202(3)	1.01(2)	

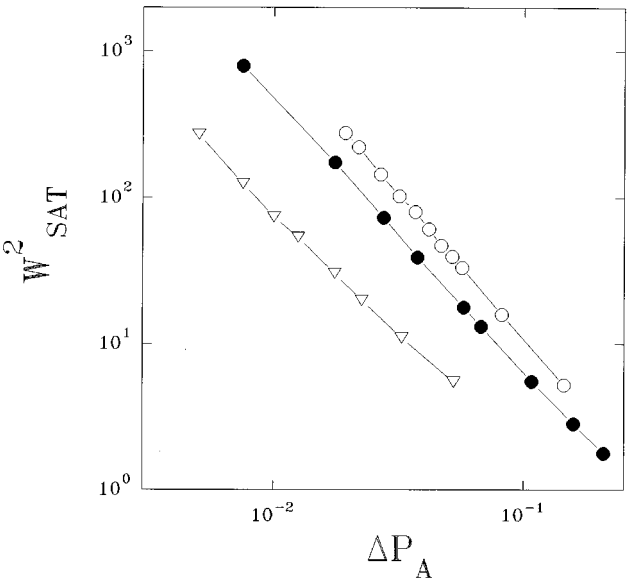

FIG. 9. Plot of the saturation value of the fluctuations in the position of the B profile w^2_{sat} (l.u.^{2}) vs ΔP_A obtained for channels of different width. From top to bottom the widths are $L=3$ l.u., $L=5$ l.u., and $L=20$ l.u.

of the front and the coverage close to the front, it could be expected that the former contribution should be negligible at the critical point. If this assumption holds, one has $\beta^* \to \frac{1}{2}$ for $L \to \infty$ pointing out that the noise should dominate over the nonlinear and surface tension terms in the KPZ equation [Eq. (5)].

On the other hand, by means of log-log plots of the saturation value of the interface width w^2_{sat} ΔP_A obtained with off-criticality, as shown in Fig. 9, it is possible to determine the exponent δ. The obtained values, evaluated from the slopes of the plots in Fig. 9, are also listed in Table I. These results also point out that δ is sensitively dependent on the channel width L, suggesting again nonuniversal behavior. The observed tendency $\delta \to 3/2$ for $L \to \infty$ has to be taken with caution since finite-lattice effects are still very strong for the used lattices $L \leqslant 20$.

If the time and pressure dependence of w^2 are well described by Eq. (10), one may expect data collapsing in log-log plots of $w^2 t^{-\beta}$ versus $t(\Delta P_A)^{\alpha}$. The excellent quality of the obtained collapsing (see Fig. 10 for $L=5$ and $L=20$) strongly suggests the validity of the scaling hypothesis involved in the derivation of Eq. (10). All these results demonstrate that the standard dynamic scaling formalism developed for the description of rough interfaces [22] is suitable for the rationalization of the interface behavior in far-from-equilibrium reactive systems.

V. CONCLUSIONS

Based on the ZGB model, a study of the displacement of poisoned phases in narrow channels is presented. Basic information on the propagation of the reactant's fronts are obtained from concentration profiles. The propagation velocities vanish at certain critical adsorption probabilities P_A^{c1} and

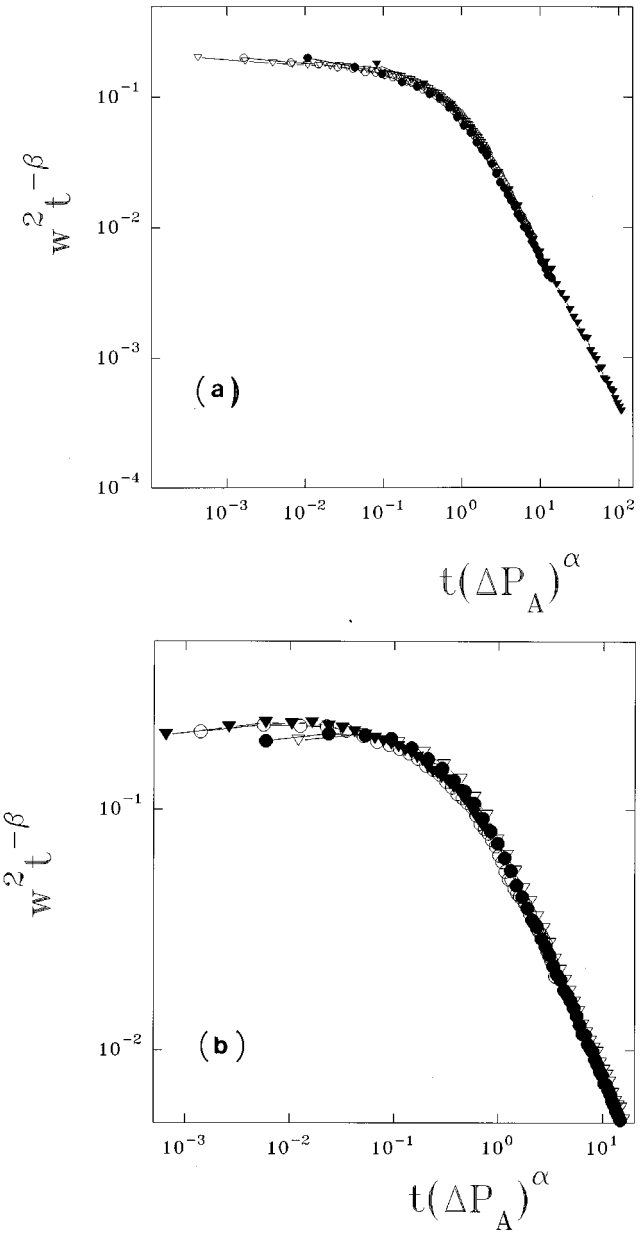

FIG. 10. Scaling plots of $w^2 t^{-\beta}$ vs $t(\Delta P_A)^{\alpha}$ obtained for channels of different width and at different adsorption probabilities. w and t are measured in l.u. and MCS, respectively. (a) $L=5$ l.u. and (b) $L=20$ l.u.

P_A^{c2}, which depend on the channel width. By means of a suitable extrapolation procedure, these probabilities are identified with the critical points of the irreversible phase transitions of the ZGB model. So, propagation of both B and A fronts occur within the (finite-size-dependent) reaction window of the ZGB model. It is found that within such a window, the interface width of B fronts diverge, but it becomes bounded for $P_A > P_A^{c2}$. The behavior of the interface width can be described using standard dynamic scaling arguments. For very narrow channels, the exponents show nonuniversal behavior, but by increasing the channel width, the value $\beta \simeq \frac{1}{2}$ is obtained, suggesting that the noise dominates the process.

Simulation results presented in this work have many points of qualitative agreement with experimental findings of front propagation reported by Haas *et al.* [13]. However, analogies have to be taken with caution because the underlaying physics should be different, since experiment may show the propagation of coexisting phases within a bistable regime. It is expected that more elaborate models, e.g., including diffusion, surface reconstruction, etc., will improve the description.

ACKNOWLEDGMENTS

This work was financially supported by the Consejo Nacional de Investigaciones Científicas y Tecnicas (CONICET) and the Universidad Nacional de La Plata, Argentina. The computer facilities used to perform this work were provided by the Volkswagen Foundation (Germany) and the Commission of European Communities under Contract No. ITDC-122.

[1] K. Christmann, in *Surface Physical Chemistry*, edited by H. Baumgartel, E. U. Franck, and W. Grunbein (Springer-Verlag, New York, 1991).
[2] V. P. Zhdanov and B. Kasemo, Surf. Sci. Rep. **20**, 111 (1994).
[3] E. V. Albano, Het. Chem. Rev. **3**, 389 (1996).
[4] P. Meakin and D. J. Scalapino, J. Chem. Phys. **87**, 731 (1987).
[5] R. Ziff, E. Gulari, and Y. Barshad, Phys. Rev. Lett. **56**, 2553 (1986).
[6] A. Maltz and E. V. Albano, Surf. Sci. **277**, 4141 (1992).
[7] E. V. Albano, Appl. Phys. A **55**, 226 (1992).
[8] J. J. Luque, F. Jiménez-Morales, and M. C. Lemos, J. Chem. Phys. **96**, 8535 (1992).
[9] J. Satulovsky and E. V. Albano, J. Chem. Phys. **97**, 9440 (1992).
[10] E. V. Albano, Surf. Sci. **235**, 351 (1990).
[11] V. D. Pereyra and E. V. Albano, Appl. Phys. A **57**, 291 (1993).
[12] M. Ehsasi *et al.*, J. Chem. Phys. **91**, 4949 (1989).
[13] G. Haas *et al.*, Phys. Rev. Lett. **75**, 3560 (1995); **76**, 1174 (1996).
[14] S. Havlin, in *The Fractal Approach to Heterogeneous Chemistry*, edited by D. Avnir (Wiley, New York, 1989), p. 251.
[15] P. Moller, K. Wetzl, M. Eiswirth, and G. Ertl, J. Chem. Phys. **85**, 5328 (1986).
[16] J. Evans and T. R. Ray, Phys. Rev. E **50**, 4302 (1994).
[17] M. Kardar, G. Parisi, and Y. C. Zhang, Phys. Rev. Lett. **56**, 889 (1986).
[18] R. H. Goodman, D. S. Graff, L. M. Sander, P. Leroux-Hugon, and E. Clément, Phys. Rev. E **52**, 5904 (1995).
[19] H. C. Kang and W. H. Weinberg, Phys. Rev. E **48**, 3464 (1993).
[20] H. C. Kang and W. H. Weinberg, J. Chem. Phys. **100**, 1630 (1994).
[21] H. C. Kang and W. H. Weinberg, Phys. Rev. E **47**, 1604 (1993).
[22] A. L. Barabási and H. E. Stanley, *Fractal Concepts in Surface Growth* (Cambridge University Press, Cambridge, 1995).